Experimental study of ELM induced fast-ion transport using passive FIDA spectroscopy at the ASDEX Upgrade tokamak

A. Jansen van Vuuren[1], B. Geiger[2], P.A. Schneider[1], K. Bogar[3], P.Zs. Poloskei[4], A. Cathey[1], M. Hoelzl[1], A.S. Jacobsen[5], M. Cavedon[1], R. Dux[1] and the ASDEX Upgrade Team[†]

[1]Max-Plank-Institut für Plasmaphysik, D-85748 Garching, Germany
[2]University of Wisconsin, WI-53706 Madison, USA
[3]Institute of Plasma Physics of the CAS, Prague, Czech Republic
[4]Max-Plank-Institut für Plasmaphysik, 17491 Greifswald, Germany
[5]Culham Science Centre, OX14 3DB Abingdon, UK
[†]See author list of H. Meyer *et al.* Nucl. Fusion **59**, 112014 (2019)

E-mail: ajvv@ipp.mpg.de

Abstract. Measurements using a recently installed edge fast-ion D-alpha (FIDA) diagnostic at the ASDEX Upgrade tokamak show a clear effect of edge localised modes (ELMs) on the passive FIDA signals. While a reduction in the passive FIDA emission is observed in the scrape-off layer (SOL) region, measurements close to the last closed flux surface show an increase in signals shortly after ELMs, followed by a decrease. The decrease provides a clear sign of fast-ion losses in the SOL, while the increase can be explained by an enhanced neutral density during ELMs inside the plasma. In addition, small ELMs are observed, which barely change the neutral density and plasma position but still cause significant changes in the passive FIDA signals. A comparison of the measurements with forward modelling shows that about 60 % of the fast ions are lost by ELMs outside the last closed flux surface. In addition, a 20 % decrease of the fast-ion density in a range up to 4 cm within the last closed flux surface can be inferred. This range agrees well with the latest modelling results of ELMs using the non-linear MHD code JOREK and shows that less than 0.3 % of all fast ions are lost by ELMs.

1. Introduction

H-mode discharges are typically accompanied by an edge instability known as the edge localised mode (ELM) [1]. The instability is driven by a characteristically steep pressure gradient and large current along the plasma edge, theoretically described by the so-called peeling-ballooning (PB) model [2]. ELMs occur quasi periodically expelling plasma from the edge, relaxing the pressure gradient and collapsing the edge kinetic profiles.

In addition to the expulsion of thermal plasma, ELMs are found to cause increased fast-ion losses as measured by fast-ion loss detectors (FILDs) at the ASDEX Upgrade (AUG) [3, 4], DIII-D and KSTAR tokamaks [5] as well as the LHD stellarator [6]. Fast-ion losses may not only degrade heating and current drive, but localised losses can also damage plasma facing components. However, measurements of the absolute level of fast-ion losses as well as the radial extent of ELM-induced modifications could not be addressed yet. Such measurements would provide important information for the development and benchmark of theories that describe the non-linear dynamics of ELMs and their impact on fusion devices' first wall.

A recently installed edge fast-ion D-alpha (FIDA) diagnostic at AUG allows to obtain information on the density and distribution of confined fast ions close to the plasma boundary. FIDA spectroscopy can be characterised as charge exchange recombination spectroscopy (CXRS) applied to investigate the distribution function of confined fast ions. The technique relies on measuring the Doppler shifted Balmer alpha emission from CX reactions between fast hydrogenic ions and donor neutrals [7]. Edge FIDA measurements on AUG contain a substantial passive contribution, particularly during off-axis neutral beam injection (NBI) heating and ELMs are observed to strongly modulate this passive FIDA emission.

This paper presents the first results on ELM-induced fast-ion redistribution, as obtained from the detailed analysis of passive FIDA emission using forward modelling. The paper is structured as follows: first an overview of a representative experiment is presented along with the diagnostic setup and measurements acquired during a window of quasi regular ELM activity. Next, the modelling of a pre and post-ELM case are discussed. Here, modelling of the fast-ion distribution functions and background neutral densities are described in detail. This is followed by results comparing the experimental and forward modelled passive FIDA spectra. Results on the magnitude and radial extent of the ELM induced fast-ion redistribution are finally presented and compared to theoretical predictions.

2. Experimental overview

2.1. Discharge overview

To investigate the impact of ELMs on the fast-ion content, a low density H-mode discharge was performed (#35681) at ASDEX Upgrade with a toroidal magnetic field B_T of $-2.5\,T$ and plasma current I_p of $0.6\,MA$. In addition to $2.5\,MW$ of central electron cyclotron resonance heating (ECRH), $5\,MW$ of off-axis NBI heating was applied to obtain a large fast-ion population at the plasma edge and thus maximise the FIDA emission in the ELM affected region. Additionally, $10\,ms$ long blips of an on-axis NBI beam were performed at $500\,ms$ intervals for ion temperature and rotation measurements.

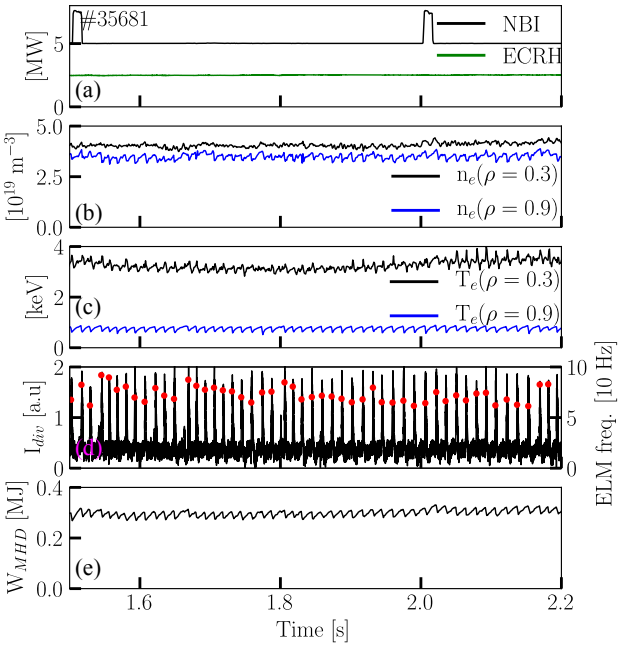

Figure 1. Time traces of the (a) heating power, (b) electron density and (c) electron temperature for discharge #35681 for the time window from 1.5 to 2.2 s. The time traces of the (d) divertor shunt current (in black) and (e) plasma stored energy for the corresponding time are also presented. The ELM frequency is plotted in red in (d).

Figure 1 shows representative time traces for a time window, from 1.5 to 2.2 s, during which the discharge exhibited quasi regular ELMs. As can be seen from figure 1b the core (in black) and edge electron density (in blue) remain relatively constant at around $4 \times 10^{19}\,m^{-3}$ and $3.5 \times 10^{19}\,m^{-3}$, respectively. The periodic drops in the edge density are a result of ELM crashes, which also strongly affect the edge electron temperature as seen (in blue) in figure 1c. The core electron temperature shows a slow moderate evolution during the time window. The periodic changes to the core electron temperature can be attributed to ELM

induced cold pulses [8].

Figure 1d shows data from the outer divertor shunt current I_{div}. The ELM crashes become apparent by spikes in the signal since heat and particles flushed out by the ELMs increase the currents flowing onto the divertor [9]. The start time of ELM crashes is defined with the onset of the rise of the I_{div} signal. The ELM frequency is observed to range between 60 and 90 Hz. This frequency range is relatively low for AUG and therefore makes this time window ideal for analysis. Furthermore, the plasma is in steady state during the roughly 50 ELMs inside the displayed time range such that the data can be synchronised with respect to the ELM onset times.

Figure 1e shows the plasma stored energy as calculated from the CLISTE [10] equilibrium reconstruction. A reduction in the plasma stored energy is seen following the ELM crashes, which is on average about 10 % of the plasma stored energy. An MHD stability analysis of the experimental edge profiles using the MISHKA code [11] has identified the ELMs as type I.

2.2. Edge FIDA setup

FIDA measurements were performed using the AUG edge FIDA system [12]. High speed measurements with exposure times of 200 µs were performed using two single channel spectrometers. In order to maximise the signal strength of the spectrometer probing the SOL region the spectrometer was connected to three adjacent lines of sight (LOS) of the edge optical system described in [13]. Bundling the LOS to a single view increases the light collection ability and improves the signal strength with the radial spot size increased from 3 mm to 9 mm.

The second spectrometer is connected to a single edge toroidal LOS from the standard FIDA system described in [14], with a radial spot size of around 1.2 cm. Importantly, the path of this LOS traverses deeper inside the plasma with its tangency radius at R =2.04 m compared to 2.12 m for the outer LOS, thus providing signal from a radially separated region. In the following, the views will be referred to as the inner and outer LOS. A poloidal projection of the views is presented in figure 2.

Figure 3 shows the regions from which passive FIDA emission is collected by the two LOS. The expected emissivity [photons] has been calculated by the FIDASIM Monte Carlo code [15] and have been mapped to the normalised radius ρ_{pol}. The broad wings arise from fast ions that are neutralised and emit Balmer alpha radiation along their path due to impact excitation. As can be seen the outer LOS collects passive FIDA emission largely from the SOL ($\rho_{pol} >$ 1.0), while the inner LOS observes passive FIDA

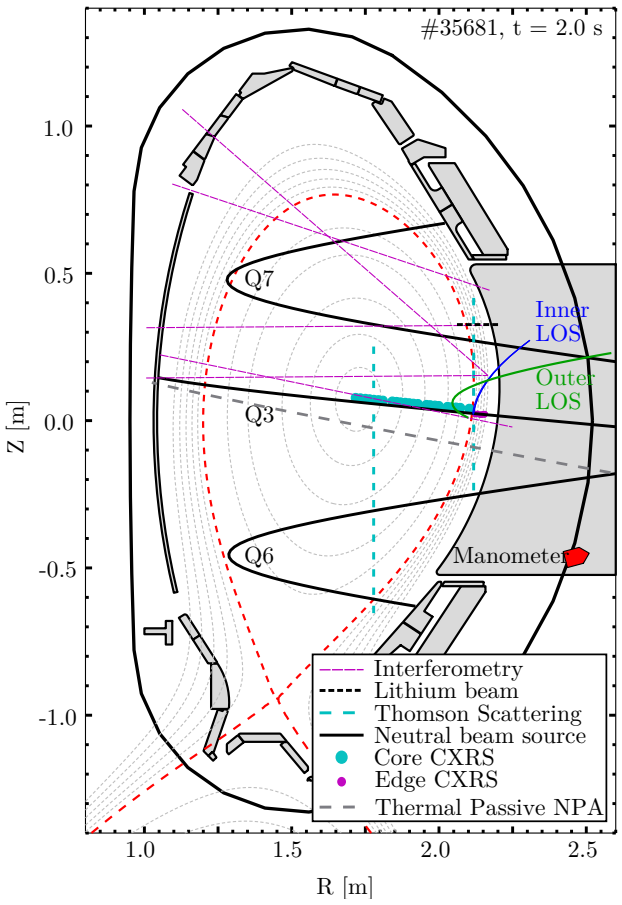

Figure 2. Poloidal view of diagnostics used for this work including the inner (blue) and outer (green) LOS connected to the high speed edge FIDA spectrometers. The views are focused on the NBI beam Q3.

emission from $\rho_{pol} \approx 0.75$ to 1.15. The difference in radial ranges probed by the two views allows for radial information to be obtained from the line integrated measurements.

Figure 4 presents the regions in fast-ion velocity-space from which passive FIDA emission is collected by the two LOS for the wavelength ranges considered in this work. These passive FIDA weight functions have been calculated using the FIDASIM code whereby the energy and pitch values of MC markers, sampled from a uniform distribution, that cross the path of the LOS and emit passive FIDA light within the given wavelength ranges are stored. As can be seen the LOS are largely sensitive to co-rotating fast ions over the selected wavelength ranges. In addition, the expected fast-ion velocity-space distribution of fast ions in discharge #35681 is shown in black. Clearly, there is a significant overlap between the weight functions and the fast-ion velocity distribution.

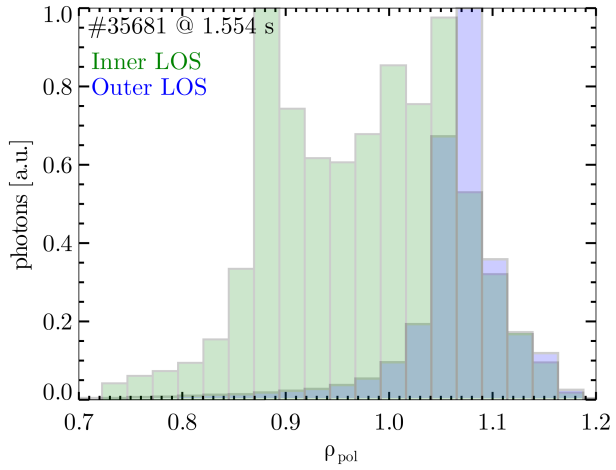

Figure 3. Comparison of the inner (green) and outer (blue) LOS passive FIDA intensity mapped to ρ_{pol}. The intensity has been normalised to the maximum emission along the respective LOS.

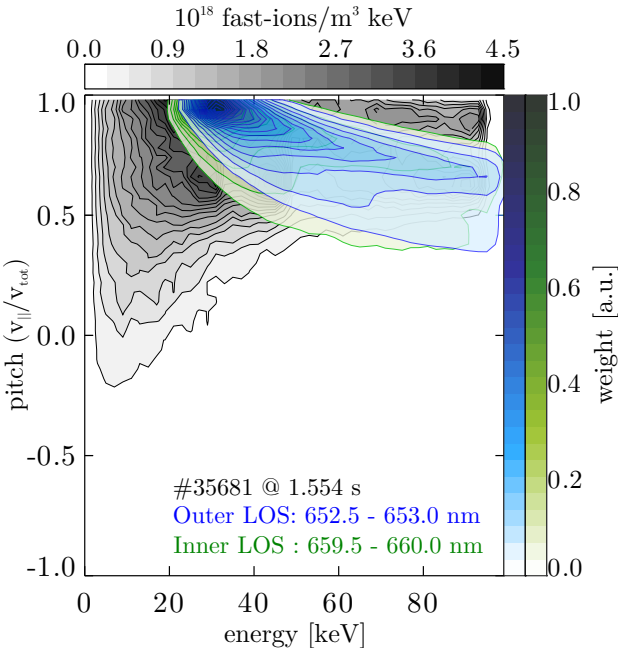

Figure 4. Passive FIDA weight functions (in colour) calculated by FIDASIM for the inner (green) and outer (blue) LOS. The grey contours illustrate a theoretical fast-ion distribution as calculated by TRANSP.

2.3. Passive FIDA measurements

Figure 5 shows the time traces of the passive FIDA emission measured for the inner and outer LOS. The Bremsstrahlung emission has been subtracted from the emission traces, which is observed in the spectrum at larger Doppler shifts than those of the FIDA radiation and which increases by $\sim$ 20 % after ELM crashes. The vertical green dashed lines mark the onset of ELM crashes which is determined from the outer

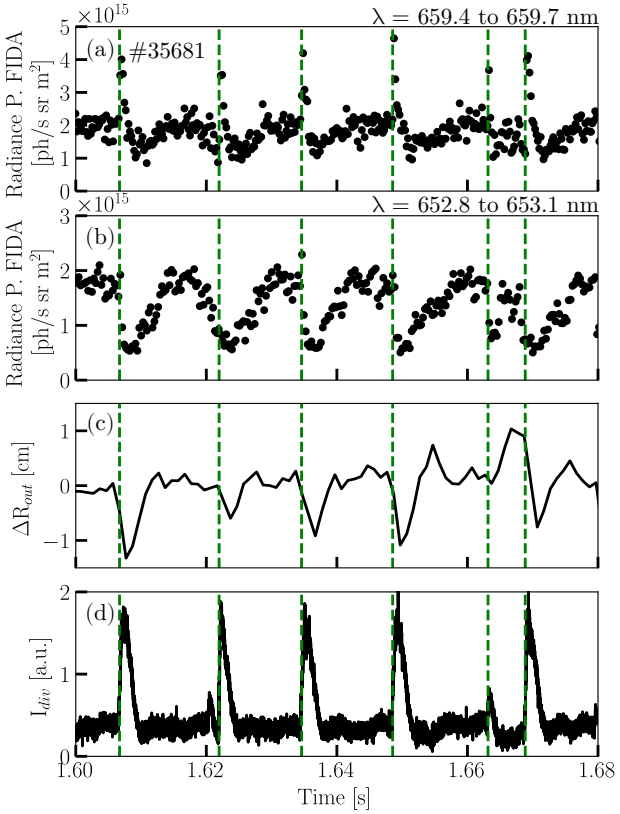

Figure 5. Time traces of the passive FIDA radiance for the (a) inner and (b) outer LOS as well as the (c) average displacement of outer most separatrix position R_{out} and (d) outer divertor shunt current. Negative ΔR_{out} indicates inward movement. The vertical green lines mark the start of ELM crashes.

divertor shunt current signal plotted in figure 5d. Figure 5c shows the time trace of the change in the outer separatrix position, with respect to the average position (R_{sep} =2.12 cm), as calculated by CLISTE. In addition, figure 6 presents the passive FIDA emission and outer separatrix position synchronised with respect to the ELM onset times. The temporal reordering is done such that 0 ms represents the ELM onset. Positive values indicate time points after the ELM crash, and negative values represent time points before the ELM crash. The rolling mean is plotted in solid red and illustrates the data trend.

The presence of ELMs is observed to have a strong modulating effect on the passive FIDA emission for both views. The emission measured along the outer LOS decreases immediately following a crash and reaches a minimum on average after around 1.5 ms at about 35 % of the pre-ELM emission intensity as seen in figure 6b. The emission thereafter increases and recovers to pre-ELM levels around 8 ms after the crash and well before the onset of the following ELM. The inner LOS on the other hand shows a sharp initial increase in the emission to more than twice the

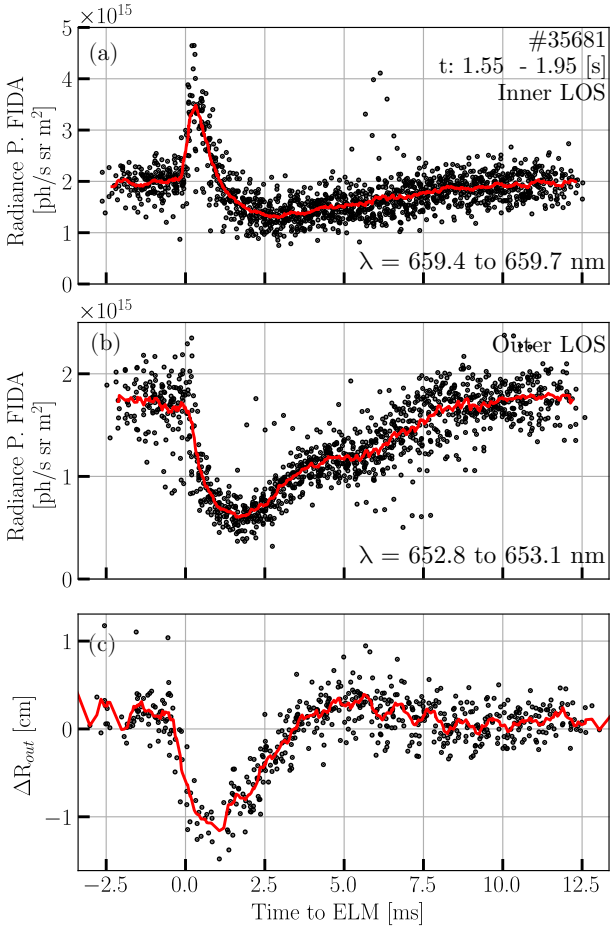

Figure 6. ELM synchronised data points of the passive FIDA radiance for the (a) inner and (b) outer LOS as well as the data points of ΔR_{out} (black). The solid red line represents the rolling average for a 0.4 ms data window.

pre-ELM intensity and peaks at around 250 µs after the ELM crash. The emission thereafter decreases strongly, reaching a minimum around 2.5 ms after the crash at about 65 % of the pre-ELM emission intensity and recovers to pre-ELM levels on a similar time scale to that of the outer view.

Figure 6c shows that the displacement of the separatrix during ELM crashes, which moves inwards by up to 1.5 cm. This affects the measured FIDA intensity as the density of fast ions along the LOS changes. However, the average recovery time of the separatrix position is only about 5 ms which is shorter than the recovery of the passive FIDA light and therefore indicates that the plasma movement does not fully account for the observed changes to the passive FIDA light. Moreover, small ELMs exist that show hardly any plasma movement but still exhibit strong changes of the passive FIDA light. Examples are the ELM at 1.62 s and another shortly after 1.66 s in fig. 5. The movement calculated in the plasma position for these times is low yet the FIDA emission over the same time period behaves similar to most other ELMs.

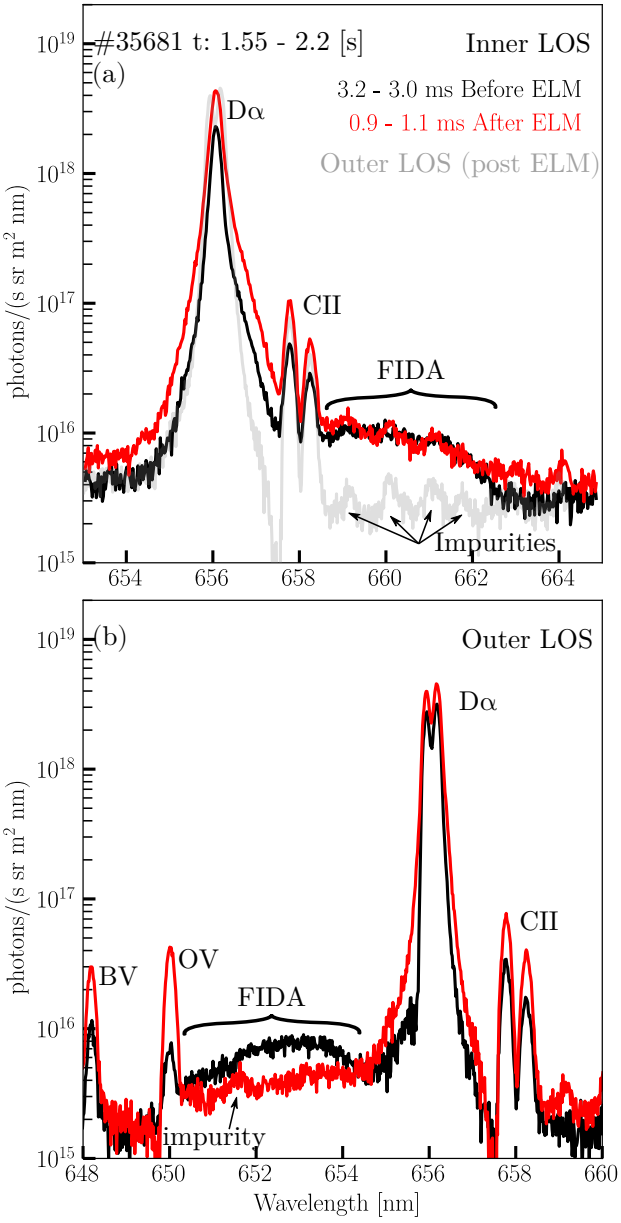

Figure 7. Conditionally averaged pre and post-ELM passive spectra, in red and black respectively, measured by the high speed edge FIDA spectrometers for the (a) inner LOS and (b) outer LOS.

Figure 7 compares the pre and post-ELM conditionally averaged spectra of the measurements presented in figure 5. The black spectrum is the average of frames −3.2 to −3.0 ms relative to the synchronised ELM crash (t_{ELM}= 0 s), while the red spectrum is the averaged spectrum of frames measured 0.9 to 1.1 ms after the ELM crash. From left to right, the spectra contains the B V (∼648 nm) and O V (650.024 nm) impurity lines followed by passive FIDA observable from about 651 to 654 nm for the outer LOS.

The emission between about 655 and 658 nm observed by both views originates from excited background neutrals whose density decays exponentially towards the plasma core. The emission exhibits intense and unshifted radiation from the cold edge neutrals and a broader feature from neutrals inside the last closed flux surface that have undergone CX reactions, which we will refer to as thermal CX emission. The double peak observed by the outer LOS for the unshifted D-alpha emission line is an instrument effect, discussed in [12], that does not affect the spectrum of the inner LOS. To the right of these contributions are two C II impurity lines at 657.805 and 658.288 nm respectively. In contrast to the outer LOS, the inner LOS observes the maximum of the passive FIDA emission, red-shifted, from about 659 to 662 nm. This difference can be explained by the mainly co-rotating fast-ion distribution function and LOS geometries that are directed into the counter-current (outer LOS) and the co-current direction (inner LOS).

A clear reduction and flattening of the passive FIDA spectrum after ELMs is observed for the outer view, accompanied by increased unshifted D-alpha as well as impurity emission lines. The inner view shows a similar increase in the unshifted D-alpha emission, while the passive FIDA emission (from about 659 to 652 nm) does not change significantly. However, it should be noted that this wavelength range contains at least four impurity emission lines as can be seen from the outer LOS post-ELM spectrum plotted in grey. The flattening of the passive FIDA indicates a possible strong impact of ELMs on the edge fast-ion distribution function along the LOS and will be quantitatively evaluated considering the effect of changes to the plasma and background neutral density through forward modelling in section 3.

2.4. Pre and post-ELM kinetic profiles

As with the spectra presented in figure 7 time coherent averaging has been applied to the electron density and temperature data acquired during the investigated time interval. The electron density n_e data is obtained from a combined Bayesian analysis [16] of the AUG interferometry system [17], the Thomson scattering (TS) system [18] and the lithium beam emission (Li-BES) diagnostic [19]. The electron temperature T_e data is obtained from the electron cyclotron emission (ECE) and the TS diagnostics. Ion temperature data is obtained from the AUG CXRS systems [20] with measurements available during the NBI beam blips.

Data during 1 ms intervals starting from 3 ms before and 1 ms after ELMs, respectively, are conditionally selected. Figure 8 shows profiles fitted to the conditionally selected data. As can be seen the post-ELM electron density is characterised by a

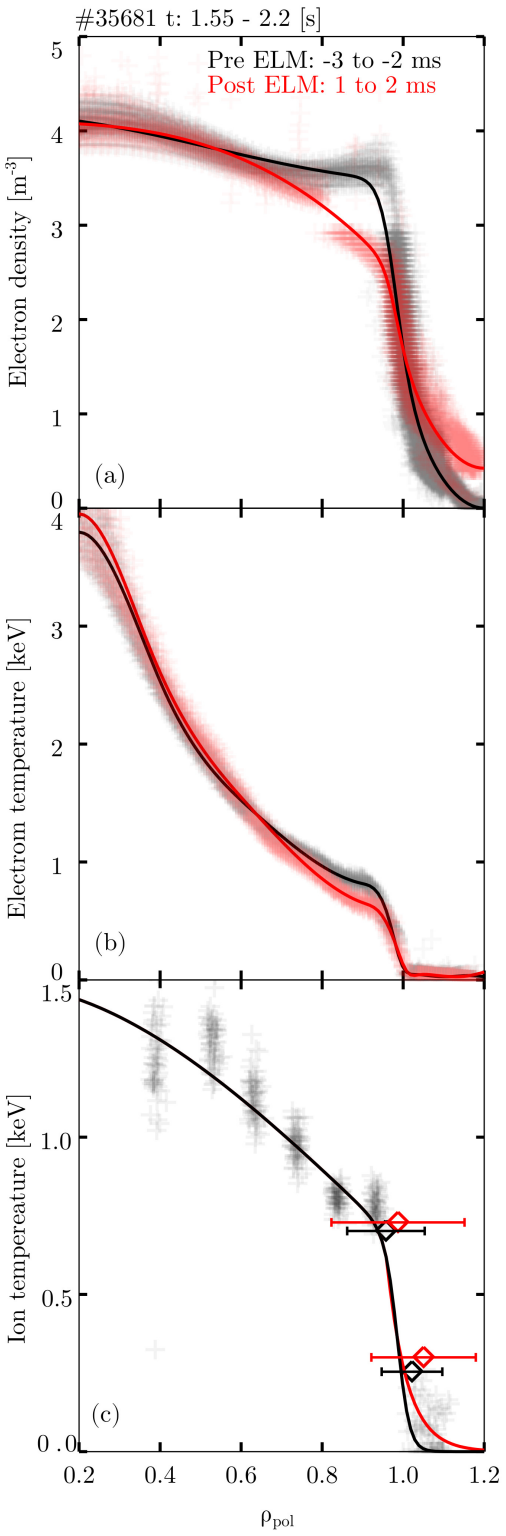

Figure 8. A comparison of the pre- (black) and post-ELM (red) profiles of the (a) electron density, (b) electron temperature and (c) ion temperature. The diamond data points represent the ion temperature obtained from fitting the passive D-alpha emission, see figure 9.

lower pedestal top value and increased SOL density. The electron temperature has a decreased pedestal top value, however, the SOL temperature is not significantly increased. ELM resolved ion temperature profiles from the CXRS data are not available for this discharge as only short 10 ms active NBI beam blips were performed. Blips are performed as the NBI source necessary for fast edge CX would corrupt the passive FIDA signal. Since the ELM period is around 15 ms no more than two ELMs occur during the beam on phases and the signal to noise ratio of the individual measurement is too low. Therefore, the ion temperature data is simply averaged over the full time interval. However, the thermal CX emission containing the FIDA spectra carries information on the ion temperature [21]. This emission has therefore been fitted in an attempt to extract ELM resolved ion temperature data for the edge.

Figure 9 shows the thermal CX emission measured along the inner view for the pre-ELM times. Two Gaussians are used to describe the passive D-alpha emission as shown in yellow and light blue. The narrow, yellow Gaussian represents radiation from electron impact excitation which is supposed to be dominant in the SOL featuring temperatures of about 20 eV (this curve has been restricted to 20eV). The broader Gaussian in light blue represents charge exchange radiation from further inside the plasma which contains information on the main-ion temperature.

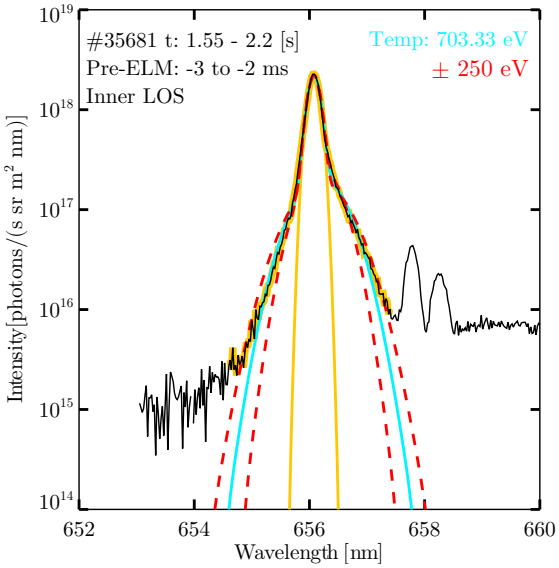

Figure 9. Double Gaussian fits to the passive, unshifted and thermal Balmer-alpha emission of the pre-ELM spectra for the inner view. The fit to the unshifted D-alpha emission is plotted in yellow and the combined unshifted and thermal CX emission in cyan from which the temperature is obtained.

The unshifted D-alpha emission has been fitted with a Gaussian restricted to 20 eV. The cyan plot represents the sum of fit to the unshifted emission and a Gaussian fit to the thermal CX data. The resulting temperatures are shown in figure 8c in addition to the profiles measured during the NBI on-phase. The temperature is found to be close to that measured by the active CXRS system. The radial position of the points have been taken where the LOS is tangential to the flux surfaces. However, as the emission is passive, the localisation of the emission is expected to be broad. The uncertainty in radial localisation is estimated using FIDASIM, with the plotted range indicating the FWHM of the calculated thermal emission. The occurrence of the data-points at different positions in ρ_{pol} is due to the inward movement of the separatrix during the ELMs considered by the equilibrium reconstruction. The measurement after the ELM crash shows slightly enhanced temperatures in the SOL region which is in line with recent results from CXRS measurements [22].

3. Modelling and Results

3.1. TRANSP modelling

TRANSP modelling has been performed to calculate the neo-classical fast-ion slowing down distribution making use of the NUBEAM module [23]. The TRANSP simulation is performed with a time step of 0.5 ms with the input data ELM synchronised in order to model a single representative ELM cycle. The simulation is performed with the input plasma current, loop voltage, major radius times toroidal magnetic field and radiated power as well as the electron temperature and density ELM synchronised. It should be noted that the ion temperature profile is kept constant during the simulation. The evolution of the separatrix position calculated by CLISTE is provided assuming only one exemplary ELM crash, along with the CLISTE pre-ELM q-profile. The simulation is initiated with the data corresponding to 5 ms before the ELM crash. The input data is kept constant for 130 ms to allow the simulation, in particular the fast-ion content, to reach a steady pre-ELM state. Thereafter the input is evolved, with the ELM crash occurring 135 ms after the start of the simulation. The resulting distribution functions from TRANSP were stored and output for the time points 3 ms before and 1 ms after the ELM crash.

Figure 10 compares the plasma stored energy calculated by CLISTE with that of TRANSP. Good agreement between the measured and predicted pre-ELM plasma stored energy level is observed. In addition, a drop of the plasma stored energy after the ELM is seen in both simulation and measurement while the simulation underestimates this drop. This is likely explained by the fact that no anomalous fast-ion

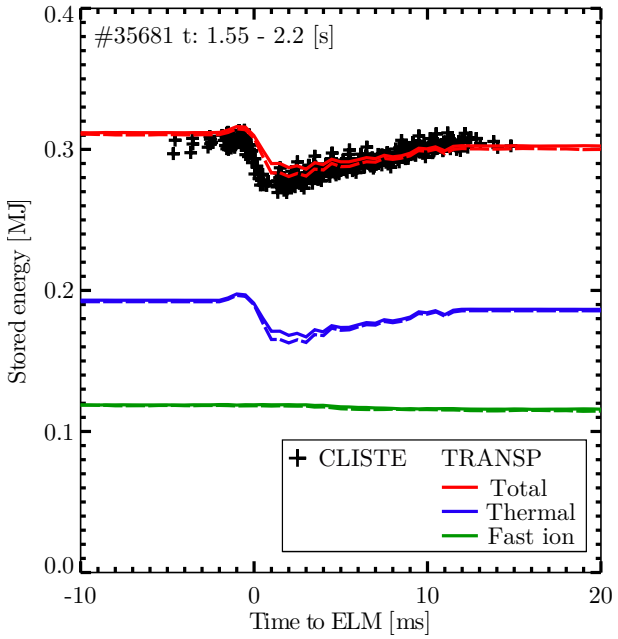

Figure 10. Time traces of the plasma stored energy as calculated by CLISTE and TRANSP. The TRANSP calculated thermal (blue) and fast ion (green) contributions are shown. The solid lines correspond to the use of a time constant T_i profile and the dashed lines to the case where $T_i \not> T_e$ during the ELM cycle.

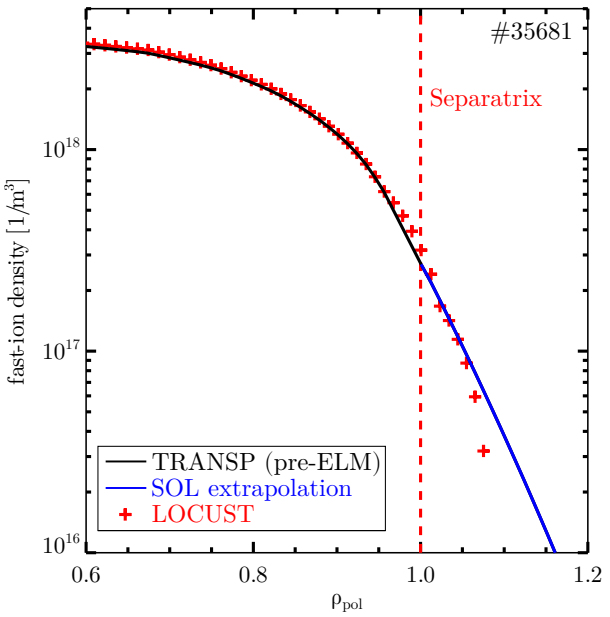

Figure 11. TRANSP calculated pre-ELM fast-ion density profile along the outer midplane. The SOL fast-ion density is extrapolated and compared to that of LOCUST.

transport was considered in TRANSP rather than pure neoclassical confinement and since the ion temperature was kept constant. To estimate the effect that changes to the ion temperature may have on the stored energy, a simulations is performed with the condition that the ion temperature profile does not exceed the electron temperature ($T_i \not> T_e$) during the ELM cycle. The result, plotted with dashed lines, is a further reduction of the post-ELM stored energy reducing the difference to the CLISTE calculated values.

In addition, simulations by the 3D fast-ion orbit following code LOCUST [24] have been performed to determine the expected SOL fast-ion density as TRANSP provides information on the fast-ion density solely for the confined region. Figure 11 shows a comparison of the (pre-ELM) outboard midplane fast-ion density profiles calculated by TRANSP and LOCUST. The TRANSP fast-ion density has been extrapolated by fitting an exponential decay function to the last two points of the profile. As can be seen the extrapolated density matches well with the LOCUST profile in the SOL. Note that we are using TRANSP for this study since TRANSP, other than LOCUST, has the ability of taking charge exchange losses into consideration.

3.2. Background neutral density characterisation

The pre and post-ELM neutral atomic D density profiles have been modelled using the 1D neutral transport code KN1D [25]. KN1D calculates the neutral density profile in slab geometry given the plasma kinetic profiles and the neutral pressure at the wall, which is treated as a free parameter. Here, we have made use of the thermal CX component in the measured FIDA spectra which contains not only information on the ion temperature (as used above) but also on the background neutral density. Forward modelling of the thermal CX emission using FIDASIM is performed to obtain a synthetic thermal emission based on the input neutral density. The latter is then scaled to match the experimental data. Constraining the neutral density is critical for the quantitative evaluation of the passive FIDA emission in the subsequent sections.

Figure 12 demonstrates how the forward modelled thermal CX emission is matched to the pre-ELM spectrum measured along the inner LOS. A similar good match is simultaneously obtained for the outer LOS suggesting that the calculated neutral density profile shape from KN1D is representative of the experimental conditions.

Figure 13 shows a comparison of the pre and post-ELM calculated neutral density profiles. Additionally, the profiles are compared to the background neutral density calculated using the technique by [26]. Hereby, the background neutral density is calculated from the passive thermal flux of neutrals as measured by neutral

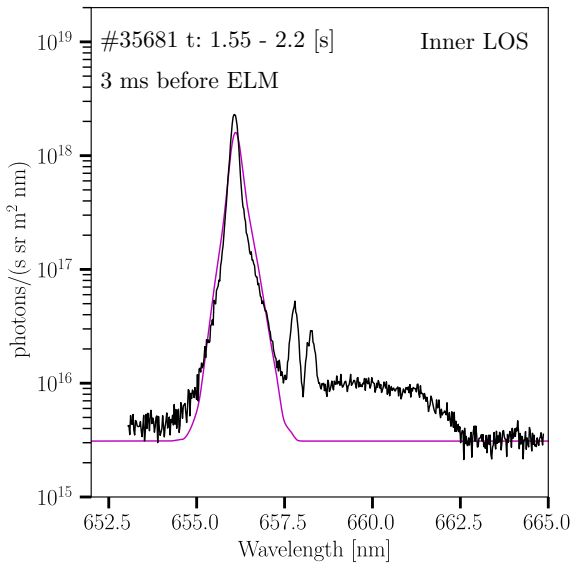

Figure 12. A comparison of the pre-ELM thermal CX emission to the measured emission along the inner LOS. The background neutral density has been scaled linearly to produce a good match to the measured spectrum.

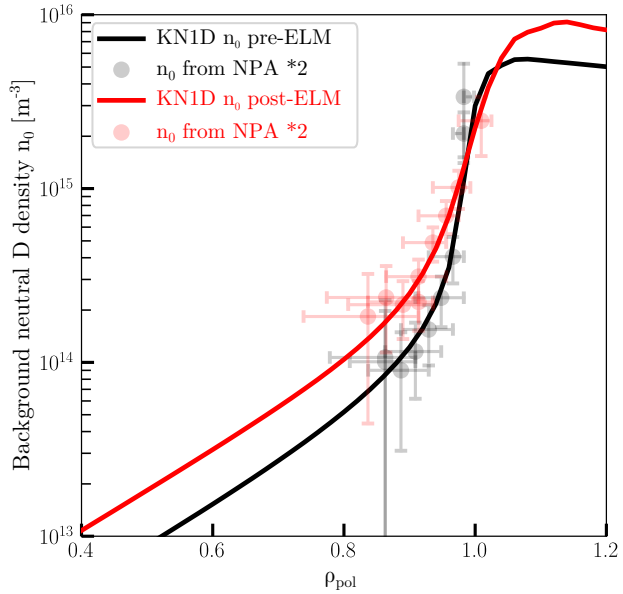

Figure 13. A comparison of the pre- (red) and post-ELM (black) background neutral D density, n_0, obtained from KN1D modelling. The n_0 calculated from the measured passive thermal flux (multiplied by a factor 2) is included as points.

particle analysers (NPA). An excellent agreement is found for the pre and post-ELM neutral density ratio comparing the constrained KN1D profiles and the NPA reconstructed densities. However, a factor of two is needed to produce an absolute match between the two methods which may be attributed to the toroidal asymmetry in the background neutral density since the two measurements are in different sectors of AUG. However, both methods show a clear increase of the core-neutral density after ELMs which likely explains the enhanced FIDA signals from the inner view. The increased post-ELM neutral density possibly results from an increased level of wall recycling following the ELM crash.

3.3. Comparison modelled spectra

Forward modelling of the passive FIDA emission is performed making use of the neutral density and fast-ion distribution functions as described above. Note here, that the inferred neutral density is also input to TRANSP to correctly treat fast-ion charge exchange losses. Figure 14 compares the FIDASIM modelled spectra for the pre-ELM case with the measured spectra for both the inner and outer views. The synthetic spectra (in magenta) includes the thermal contribution. For the outer LOS a good match between the synthetic and measured spectrum is observed. Only around 655 nm there is a slight mismatch, most likely due to a camera readout error discussed in [12], where a decrease in the measured counts is seen to the left of strong emission peaks.

The synthetic spectrum calculated for the inner LOS slightly underestimates the measured FIDA component above 660 nm. This discrepancy can, in part, be attributed to additional line radiation from impurity lines and in part by a modified or larger fast-ion population than what is expected from TRANSP. Note here that the wavelength range above 660 nm corresponds to fast ions with energies above 33 keV.

Figure 15 shows measured and synthetic spectra for the post-ELM case. The good match between the thermal CX emission and the modelling results is explained by the afore-discussed method of determining the neutral density. For the outer LOS, the synthetic passive FIDA emission is significantly larger than the measured one. This overestimation can likely be attributed to ELM-induced fast-ion losses, not considered by the neoclassical fast-ion distribution function from TRANSP. Note here, that this result already considers the radial plasma movement during ELMs mentioned before in section 2. The inner LOS does not show a similarly large over-estimation of the FIDA emission after the ELM crash. However, the FIDA wavelength range contains several impurity emission lines that contaminate the emission. Comparing the measured and synthetic emission around 659.5 nm, a region between two impurity lines, does indeed indicate there is a minor over-estimation of the FIDA emission for the inner LOS.

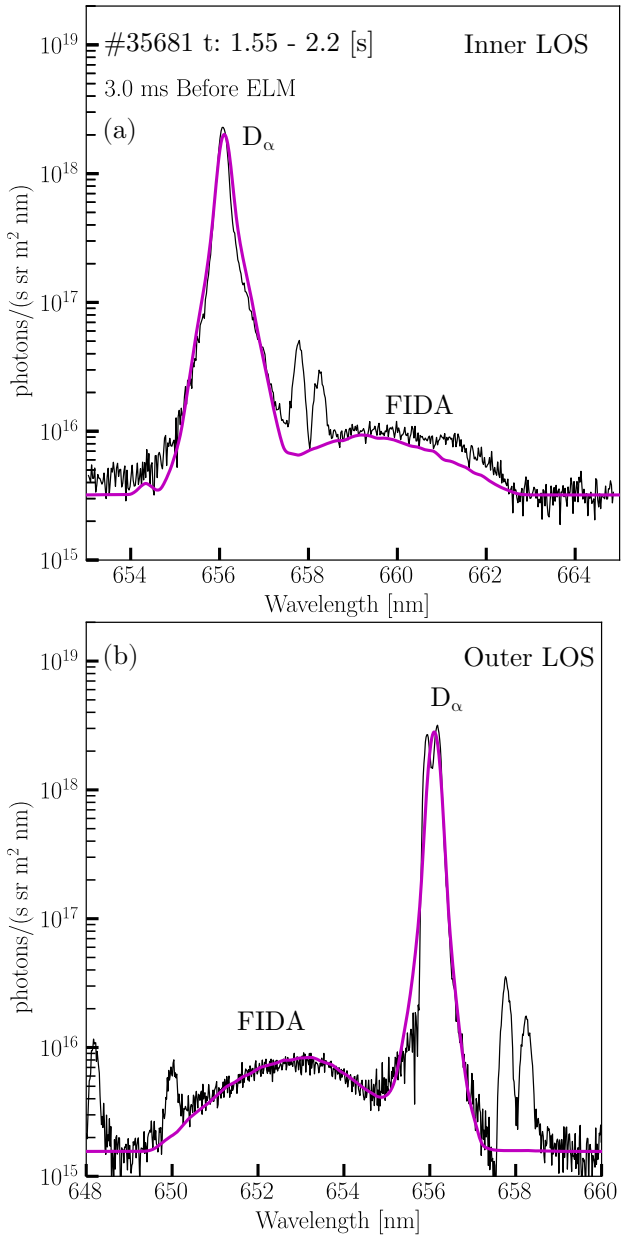

Figure 14. Pre-ELM averaged spectra (in black) compared to synthetic spectra (in magenta) calculated using FIDASIM for the (a) inner and (b) outer LOS.

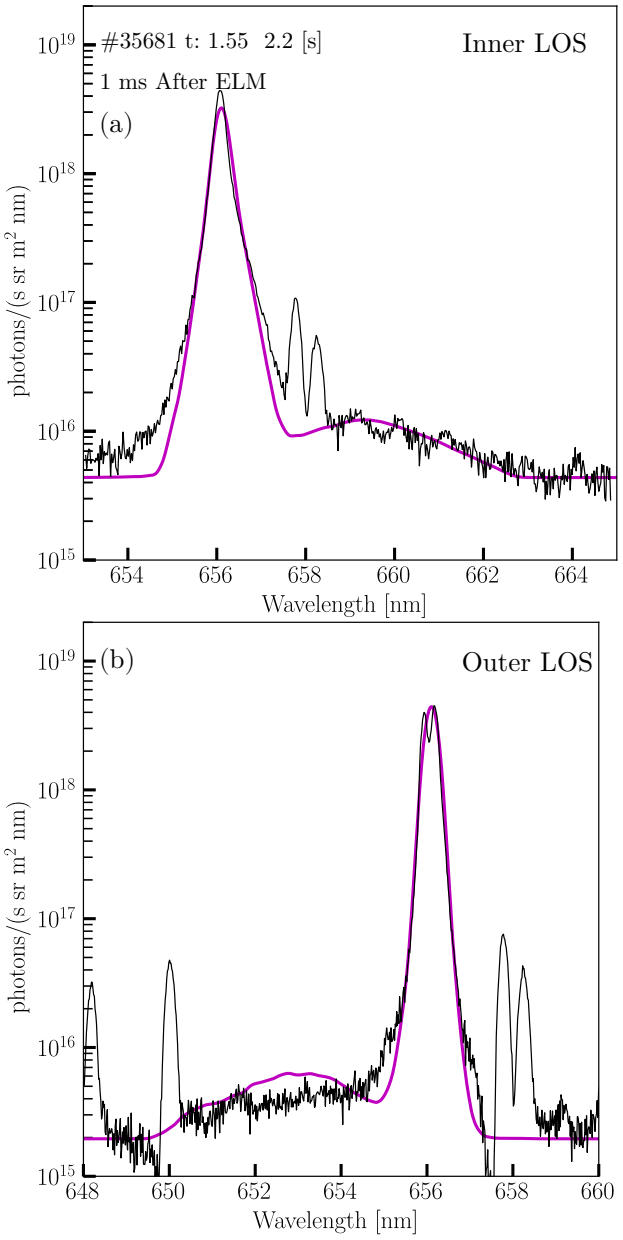

Figure 15. A comparison of the conditionally averaged post-ELM passive spectra to the FIDASIM calculated spectra for the (a) outer and (b) inner LOS.

3.4. Modification of the fast-ion distribution function

To estimate the quantity of fast ions ejected and the radial region affected by ELM crashes, a scan is performed whereby the TRANSP post-ELM fast-ion density profile is modified in height (Δn_{fast}) and over a radial range starting outside the plasma up to the separatrix position plus ΔX. Figure 16 demonstrates such modifications to the fast-ion density starting from $\Delta X = 2\,\mathrm{cm}$ inside the separatrix and extending outwards. The fast-ion density is uniformly reduced in increments of 20 % from 0 to 100 %. The innermost starting position of the region modified (ΔX) is scanned by incrementally moving outwards in steps of 1 cm, from 6 to $-4\,\mathrm{cm}$, where positive values mark positions inside the separatrix and negative values positions outside. It should be noted that the fraction of particles removed is uniform with respect to pitch and energy. Therefore, the velocity space dependence of the ELM induced fast-ion redistribution is not considered here.

Figure 17 presents for instance the FIDASIM calculated spectra for modifications of ΔX =0 cm for both LOS. The synthetic spectra are plotted in

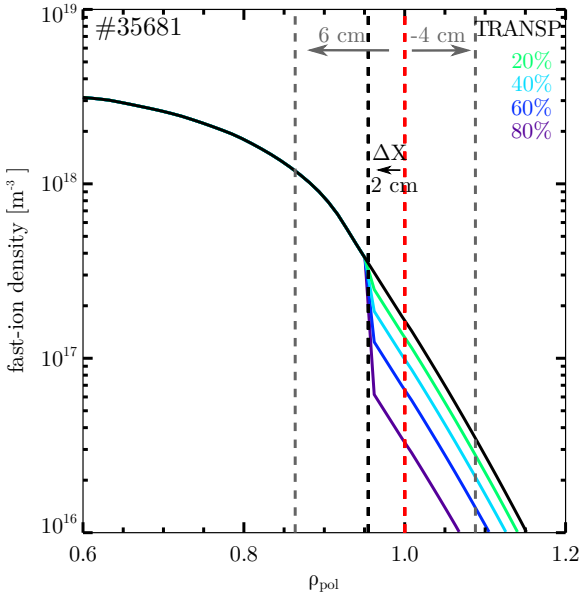

Figure 16. A scan of modifications to the TRANSP post-ELM fast-ion density profile (black). Modifications extend outwards from ΔX =2 cm marked by the vertical black dashed line. The scan range of ΔX is indicated by the vertical grey lines. The coloured profiles represent modifications where the density is reduced by increments of 20 %.

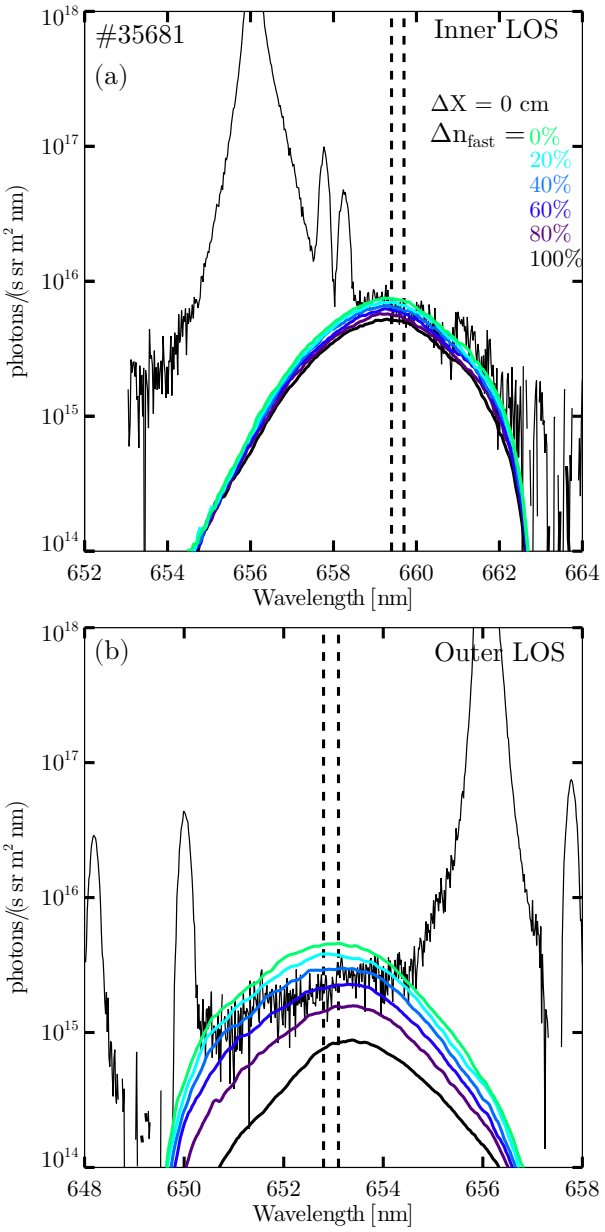

Figure 17. A comparison of the post-ELM measured spectra to the synthetic spectra obtained from the scan of the modifications to fast-ion density profile presented in figure 16, for the (a) inner and (b) outer LOS. The vertical dashed lines indicate the wavelength range over which the comparison against the measured spectra is made.

different colours corresponding to the percentage of particles removed. The green spectra labelled 0 % represents the unmodified TRANSP post-ELM case. For an increasing amount of particles removed the calculated passive FIDA intensity decreases. The outer view is more susceptible to changes in the SOL fast-ion density, as compared to the inner view. This can be explained by the spatial regions probed by the two LOS as presented in figure 3. Here the best match between the calculated and measured spectrum is a reduction of 60 % of the SOL fast-ion density for the outer view and a reduction in the range of 20 to 60 % for the inner LOS.

Figure 18 presents a 2D overview of the degree of agreement between the measured and modelled spectra as a function of ΔX and the modified percentage (Δn_{fast}). Black represents the best agreement between the measured and synthetic spectra describing an absolute difference of less than 5 %. The relative uncertainty of the measured passive FIDA emission over the compared wavelength range is on the order of 15 % for the outer view, while for the inner view it is around 5 %. Therefore the purple coloured contours correspond to synthetic spectra falling within the uncertainty for the outer LOS, while the black coloured contours falls within the uncertainty for the inner LOS.

Figure 18 shows that for the outer view the best match to spectra corresponds to a 60 % reduction of fast-ion content with ΔX =0, i.e. from the separatrix increasing for modifications to radial locations further outside. As the outer LOS does not probe significantly deeper than the separatrix, modifications to the fast-ion density extending further into the plasma reveals no additional radial information. The depth of ELM induced modifications can be inferred from the comparison with the inner LOS. A reduction of 20 % of the particles up to 4 cm matches the ELM induced

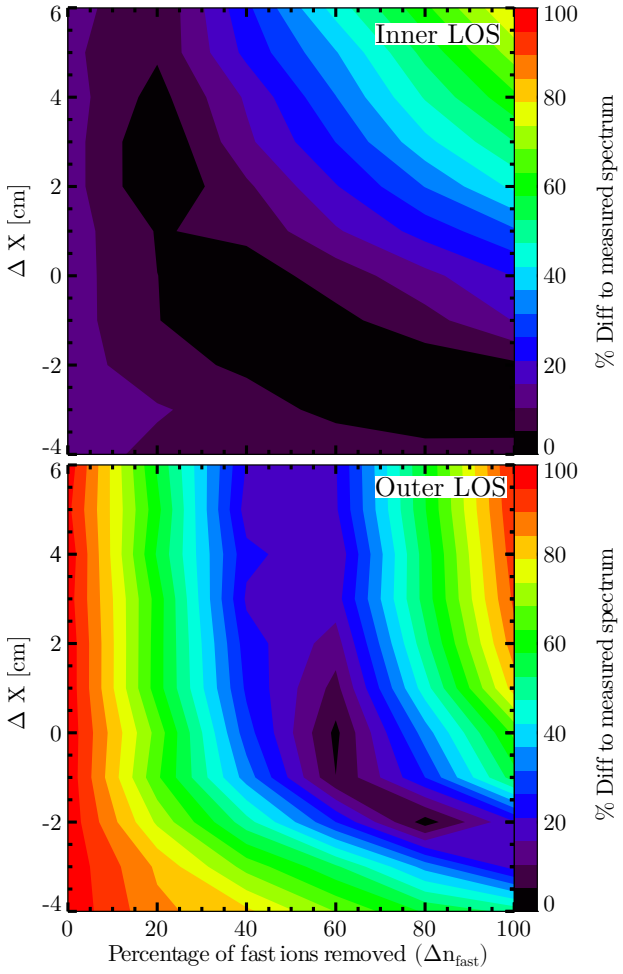

Figure 18. Results from the comparison of the measured post-ELM passive FIDA radiance to the synthetic passive FIDA calculated from the scan of modifications to the fast-ion density profile for the (a) inner and (b) outer LOS.

change in emission intensity of the inner LOS. The corresponding amount of fast ions lost with respect to the total fast-ion content is calculated to be less than 0.3 %. This corresponds to a loss of less than 1 % of the fast-ion stored energy with respect to the pre-ELM total and roughly agrees with the remaining small difference between the TRANSP simulation and the measured plasma stored energy which can be mainly attributed to changes of the ion temperature.

This result agrees with recent non-linear simulations of type-I ELM crashes with JOREK [27]. For a comparable AUG experiment it is found that the connection length is significantly decreased during ELM crashes up to $\rho_{\mathrm{pol}} \sim 0.9$. For passing fast ions that more roughly follow along field-lines, this translates to ELM-induced losses up to the same radius inside the plasma and therefore agrees with our observation.

4. Summary

High speed measurements of Balmer emission viewed along two edge LOS show ELM correlated modulation of the passive FIDA intensity. The pre-ELM passive FIDA emission at the edge could be well modelled with a neo-classical fast-ion distribution calculated by TRANSP and using neutral density profiles inferred by KN1D and scaled based on the measured thermal charge exchange emission contained in the FIDA spectra. Post-ELM modelling addressed both the change in neutral density and movement of the plasma separatrix as a result of the ELM. Kinetic profile changes of the n_{e}, T_{e}, T_{i} largely influence the FIDA signal indirectly via changes to the background neutral density. The post-ELM background neutral density, constrained against the thermal CX emission, is found to increase significantly within about 1 ms after the ELM. This is in good qualitative agreement with the neutral density inferred from neutral particle analysers. In particular in the SOL plasma, the measured FIDA signal is significantly reduced which could mainly be attributed to fast-ion losses. To quantify both the absolute losses and the radial extent of modifications to the fast-ion distribution a scan is performed removing particles in a step like manner. Comparing the FIDASIM calculated spectra to the measured spectra shows that a reduction of 60 % of the SOL fast-ion content and 20 % of the fast-ion content up to 4 cm inside the separatrix best agree with measurements. This is less than 0.3 % of the total fast-ion content. The ELM affected region is found to be up to 4 cm inside the separatrix which is in good agreement with the radial extent of modifications to the connection length calculated by a simulation of an ELM crash using the nonlinear MHD code JOREK.

Acknowledgements

This work has been carried out within the framework of the EUROfusion Consortium and has received funding from the Euratom research and training programme 2014-2018 and 2019-2020 under grant agreement No 633053. The views and opinions expressed herein do not necessarily reflect those of the European Commission.

[1] H. Zohm. Edge localized modes (ELMs). *Plasma Physics and Controlled Fusion*, 38(2):105–128, Feb 1996.

[2] J. W. Connor, A. Kirk, and H. R. Wilson. Edge localised modes (elms): Experiments and theory. *AIP Conference Proceedings*, 1013(1):174–190, 2008.

[3] M. García-Muñoz et al. Fast-ion losses induced by ELMs and externally applied magnetic perturbations in the ASDEX Upgrade tokamak. *Plasma Physics and Controlled Fusion*, 55(12):124014, Nov 2013.

[4] J. Galdon-Quiroga, M. Garcia-Munoz, K.G. McClements, M. Nocente, S.S. Denk, S. Freethy, A.S. Jacobsen, F. Orain, J.F. Rivero-Rodriguez, M. Salewski, L. Sanchis-Sanchez, W. Suttrop, E. Viezzer, M. Willensdorfer, and and. Observation of accelerated beam ion population during edge localized modes in the ASDEX upgrade tokamak. *Nuclear Fusion*, 59(6):066016, may 2019.

[5] M. García-Muñoz et al. Fast-ion redistribution and loss due to edge perturbations in the ASDEX Upgrade, DIII-D and KSTAR tokamaks. *Nuclear Fusion*, 53(12):123008, Nov 2013.

[6] Kunihiro Ogawa, Mitsutaka Isobe, Kazuo Toi, Akihiro Shimizu, Donald A Spong, Masaki Osakabe, and Satoshi Yamamoto and. Energetic ion losses caused by magnetohydrodynamic activity resonant and non-resonant with energetic ions in large helical device. *Plasma Physics and Controlled Fusion*, 56(9):094005, aug 2014.

[7] W W Heidbrink, K H Burrell, Y Luo, N A Pablant, and E Ruskov. Hydrogenic fast-ion diagnostic using Balmer-alpha light. *Plasma Physics and Controlled Fusion*, 46(12):1855–1875, nov 2004.

[8] E Trier, E Wolfrum, M Willensdorfer, Q Yu, M Hoelzl, F Orain, F Ryter, C Angioni, M Bernert, M G Dunne, S S Denk, J C Fuchs, R Fischer, P Hennequin, B Kurzan, F Mink, A Mlynek, T Odstrčil, P A Schneider, U Stroth, G Tardini, B Vanovac, and and. ELM-induced cold pulse propagation in ASDEX upgrade. *Plasma Physics and Controlled Fusion*, 61(4):045003, feb 2019.

[9] A. Kallenbach et al. Divertor power and particle fluxes between and during type-I ELMs in the ASDEX Upgrade. *Nuclear Fusion*, 48(8):085008, Jul 2008.

[10] W. Schneider et al. ASDEX Upgrade MHD equilibria reconstruction on distributed workstations. *Fusion Engineering and Design*, 48(1):127 – 134, 2000.

[11] A. B. Mikhailovskii, G. T. A. Huysmans, W. O. K. Kerner, and S. E. Sharapov. Optimization of computational mhd normal-mode analysis for tokamaks. *Plasma Physics Reports*, 23(10):844–857, 1997.

[12] A. Jansen van Vuuren et al. An edge fast-ion d-alpha system installed at ASDEX Upgrade. *Review of Scientific Instruments*, 90(10):103501, 2019.

[13] M. Cavedon, T. Pütterich, E. Viezzer, R. Dux, B. Geiger, R. M. McDermott, H. Meyer, U. Stroth, and the ASDEX Upgrade Team. A fast edge charge exchange recombination spectroscopy system at the ASDEX Upgrade tokamak. *Review of Scientific Instruments*, 88(4):043103, 2017.

[14] B. Geiger et al. Fast-ion D-alpha measurements at ASDEX Upgrade. *Plasma Physics and Controlled Fusion*, 53(6):065010, Apr 2011.

[15] B. Geiger, L. Stagner, W.W. Heidbrink, R. Dux, R. Fischer, Y. Fujiwara, A.V. Garcia, A. S. Jacobsen, A. Jansen van Vuuren, A. N. Karpushov, D. Liu, P. A. Schneider, I. Sfiligoi, P. Zs. Poloskei, and M. Weiland. Progress in modelling fast-ion d-alpha spectra and neutral particle analyzer fluxes using FIDASIM. *Plasma Physics and Controlled Fusion*, 62(10):105008, aug 2020.

[16] R. Fischer et al. Integrated data analysis of profile diagnostics at ASDEX Upgrade. *Fusion Science and Technology*, 58(2):675–684, 2010.

[17] A. Mlynek et al. Design of a digital multiradian phase detector and its application in fusion plasma interferometry. *Review of Scientific Instruments*, 81(3):033507, 2010.

[18] H. Murmann, S. Götsch, H. Röhr, H. Salzmann, and K. H. Steuer. The Thomson scattering systems of the ASDEX Upgrade tokamak. *Review of Scientific Instruments*, 63(10):4941–4943, 1992.

[19] M. Willensdorfer et al. Characterization of the Li-BES at ASDEX Upgrade. *Plasma Physics and Controlled Fusion*, 56(2):025008, Jan 2014.

[20] R. M. McDermott et al. Extensions to the charge exchange recombination spectroscopy diagnostic suite at ASDEX Upgrade. *Review of Scientific Instruments*, 88(7):073508, 2017.

[21] B. A. Grierson, K. H. Burrell, W. W. Heidbrink, M. J. Lanctot, N. A. Pablant, and W. M. Solomon. Measurements of the deuterium ion toroidal rotation in the diii-d tokamak and comparison to neoclassical theory. *Physics of Plasmas*, 19(5):056107, 2012.

[22] M. Cavedon et al. Pedestal and er profile evolution during an edge localized mode cycle at ASDEX Upgrade. *Plasma Physics and Controlled Fusion*, 59(10):105007, Aug 2017.

[23] A. Pankin, D. McCune, R. Andre, G. Bateman, and A. Kritz. The tokamak Monte Carlo fast ion module NUBEAM in the National Transport Code Collaboration library. *Computer Physics Communications*, 159(3):157 – 184, 2004.

[24] R. J. Akers, E. Verwichte, T. J. Martin, S. D. Pinches, and R. Lake. GPGPU Monte Carlo calculation of gyro-phase resolved fast ion and n-state resolved neutral deuterium distributions. In *Proc. 39th EPS Conference on Plasma Physics*, page P5, 2012.

[25] B LaBombard. KN1D: A 1-D space kinetic, 2-D velocity, transport algorithm for atomic molecular hydrogen in an ionizing plasma. Research Report PSFC-RR-01-3, Massachusetts Institute of Technology, Plasma Science and Fusion Center, 175 Albany St., Cambridge, MA 02139 USA, 2001.

[26] K. Mitosinkova et al. Direct determination of background neutral density profiles from neutral particle analyzers. In *45th EPS Conference on Plasma Physics*. European Physical Society, 2018.

[27] A. Cathey et al. Non-linear extended MHD simulations of type-I edge localised mode cycles in ASDEX Upgrade and their underlying triggering mechanism. *Nuclear Fusion*, Submitted.